lubricants

Article

Numerical Analysis for Wetting Behaviors of an Oil Jet Lubricated Spur Gear

Yu Dai, Chongyu Liang, Xi Chen and Xiang Zhu *

College of Mechanical and Electrical Engineering, Central South University, Changsha 410083, China; 210143@csu.edu.cn (Y.D.); 203712174@csu.edu.cn (C.L.); 213712157@csu.edu.cn (X.C.)
* Correspondence: zhuxiang_csu@163.com

Abstract: As it is widely employed in the aeronautical transmission system, a better understanding of the oil jet lubrication behavior is vital to determine the total system energy consumption. Firstly, this study presents related theoretical models such as the sum of oil jet resistance torque, impingement depth, and wetted area of the oil film for calibrating the physical characteristics of the impact of the oil jet on the gear flank. Then, in terms of the flow phenomenology of the liquid column for the oil jet impact on an isolated spur gear, a detailed transient and spatial flow field analysis becomes available, benefiting from an overset mesh method integrating with a volume-of-fluid (VOF) method. Furthermore, not only the oil jet resistance torque, but also the impingement depth as well as the spatial and temporal evolution of wetted surface by the oil film on the gear tooth given by numerical investigations were compared well with the theoretical calculations.

Keywords: oil jet; windage; resistance loss; overset method; CFD; spur gear

Citation: Dai, Y.; Liang, C.; Chen, X.; Zhu, X. Numerical Analysis for Wetting Behaviors of an Oil Jet Lubricated Spur Gear. *Lubricants* **2022**, *10*, 17. https://doi.org/10.3390/lubricants10020017

Academic Editor: Lars-Göran Westerberg

Received: 6 December 2021
Accepted: 18 January 2022
Published: 20 January 2022

1. Introduction

Motivated by severe GHG (greenhouse gas) emissions nowadays, the aircraft industry is committed to reducing energy consumption, thereby continuously improving the transmission efficiency of each gearing system in the aeroengine. Even though the gearbox can have an efficiency of more than 99% [1], the power losses (i.e., no-load losses and load losses) are still considerable in a magnitude 100 MW application [2]. The load losses of gears are tied to the friction behavior of gear mesh, namely a mechanical power loss, whereas the no-load losses are associated with motions of lubricant and air. The latter is far from negligible at high speeds [3].

Two common lubrication methods are splash lubrication and oil jet lubrication. The no-load losses of dipped lubricated gears mainly include fluid trapping and squeezing power losses, and churning power losses [4–7]. For jet-lubricated gears, there are other losses—impulse power losses and windage power losses, without churning losses [8,9]. The impulse power losses are related to the momentum transfer when the high-speed oil stream injected from the oil jet nozzle impacts the gear tooth surface. In a high-speed gearing system, it is of significance to estimate the impulse losses with jet lubrication during the design of gearboxes, considering the effects of geometry and working parameters. As an example, Ariura et al. [10] have measured the impulse power losses of a spur gear system with oil jet lubrication; their results suggested that the impulse power losses consist of the power required to trap and accelerate the oil jet flow in the tooth space. The windage power losses are associated with the pure air or air–lubricant pumping by the gear; especially in the air–oil mixture, the gear suffers from a considerable windage power losses [11–14].

A pioneering study was conducted by Akin and his colleagues to firstly introduce impingement depth on the gear tooth for predicting the lubrication and cooling performance [15]. They also conducted experiments to validate the theoretical depth models and pointed out that an optimal oil nozzle layout can provide a maximum impingement depth, bringing better cooling effect. Similar studies were submitted by Dai et al.; they investigated not only the penetrating depth on spur/helical gear pairs [16], but also spiral bevel gears [17] and face gears [18]. These scholars emphasized the relationship between the nozzle layout and the theoretical impingement, but neglected the resistance torque or the impulse power losses due to the action of oil flow impacting the gear surface.

Computational fluid dynamics (CFD) is capable of providing a more in-depth understanding of the oil/air flow and the associated power losses [19,20], and could describe the fluid-dynamical phenomenon easily and accurately [21–24]. There are limited numerical studies on oil jet behavior owing to the multiphase flow, complex gear structure, and tiny oil flow. Fondelli et al. [25] investigated an oil flow impacting on a spur gear by leveraging with the sliding mesh method. The corresponding resisting torque was obtained, and the oil–gear interaction was categorized into four phases accordingly. The numerical results reveal a good agreement with the theoretical resistance torque based on the momentum theorem during the oil–gear interaction. Furthermore, they [26] explored the influence of injection angle on the resistant torque; the results show that the increase in the oil jet angle along with the gear rotation contributes to the decreases in the average resisting torque, consistent with the algebraic model. A similar study by Keller et al. [27] is also reported utilizing the sliding mesh method; it should be noted that the greatest innovation was the use of five teeth instead of the whole gear for its oil jet lubrication analysis. Additionally, the impact behavior of an oil jet on a spinning gear has been investigated via smoothed particle hydrodynamics (SPH) [28,29], SPH is the most promising method in terms of superior performance regarding computational effort and suffering from a lack of accuracy. Besides, on the basis of the definition of the impingement depth, Kormer et al. [30,31] developed an analytical model for quantifying the heat transfer convection coefficient of the oil film on the spur gear under jet lubrication, well in accordance with experimental facts.

For the moment, it is difficult to assess the oil jet power loss of the impact of the oil jet flow on the gear flanks owing to its persistent short time. With regard to the design practice and computational efforts, the oil jet behavior of the whole gear instead of a few gears is more commonly invetigated. Therefore, this study first introduces the relevant theoretical models to provide a deep understanding of the flow characteristics of the oil jet lubrication for an isolated spur gear, allowing a measure of key parameters. More than that, however, by leveraging an overset method integrating with the VOF method, the jet flow of flow phenomenology can also be available. Subtracting the windage effects, the comparison of the theoretical calculations with the numerical results was then performed for the whole spur gear.

2. Theoretical Model

The investigated oil flow impacting on the gear tooth relates to some basic formulations of gear motions explained subsequently.

2.1. Oil Jet in Crossflow

The lubricating oil flies from the nozzle and crosses the airflow surrounding the rotating gear. The current flow phenomenon can be transferred to a problem of an oil jet in crossflow. The circumferential airflow velocity is equal to the same order of magnitude of the pitch line velocity ($U_{air} \approx 0.9U_p$), following the description of Fondelli et al. [25]. The empirical formula was proposed to predict the travel distance yd of the liquid column before breaking up into droplets in a cross flow, as derived by Wu et al. [32,33]:

$$\frac{y_d}{d_j} = 3.07q^{0.53} \tag{1}$$

where q is the oil to air momentum ratio.

$$q = \frac{\rho_{oil} U_j^2}{\rho_{air} U_{air}^2} \tag{2}$$

where ρ_{oil} and ρ_{air} are the density of oil and air, respectively. U_j is the oil jet velocity. Equations (1) and (2) were applied for the operating conditions in this paper. Equation (1) integrating with Equation (2) is capable of estimating the travel distance, while the Weber number characterizes the regimes of liquid breakup.

$$\mathrm{We}_{\mathrm{cf}} = \frac{\rho_{air} {U_{air}}^2 d_j}{\sigma} \tag{3}$$

where σ represents the surface tension coefficient of oil. The calculated travel distance y_d is clearly far greater than the small distance from nozzle exit to the outside diameter of the gear (l_o = 12.5 mm). The subatmospheric pressure results in the decrease in air density as well as the aerodynamic forces exerting on the oil jet flow (q = 226 and W_{ecf} = 22); no significant oil jet breakup or deflection occurs before impacting on the gear surface.

2.2. Oil Jet Resistance Torque

A simple analytical model, developed by Fondelli [25,26], can estimate the resistance torque in the presence of oil jet lubrication. With regard to Figure 1, the oil is accelerated up to the pitch-line velocity by the rotating airflow as it approaches the gear. The resistance torque can be expressed as

$$T_j = \frac{\pi}{4\omega_g} \rho_{oil} U_j U_p \left(d_j\right)^2 \left(U_p - U_j \sin\beta\right) \tag{4a}$$

where ρ_{oil} is the oil density; ω_g denotes the gear's angular speed; U_p and U_j are the velocity of the pitch line and oil jet, respectively; and β is the oil jet angle for $\beta > 0$ in the rotation direction (right), and vice versa, see Figure 2. This study considered that only the oil jet angle β is set to zero, so the resistance torque can be simplified as

$$T_0 = \frac{\pi}{4} \rho_{oil} \omega_g U_j \left(R_p d_j\right)^2 \tag{4b}$$

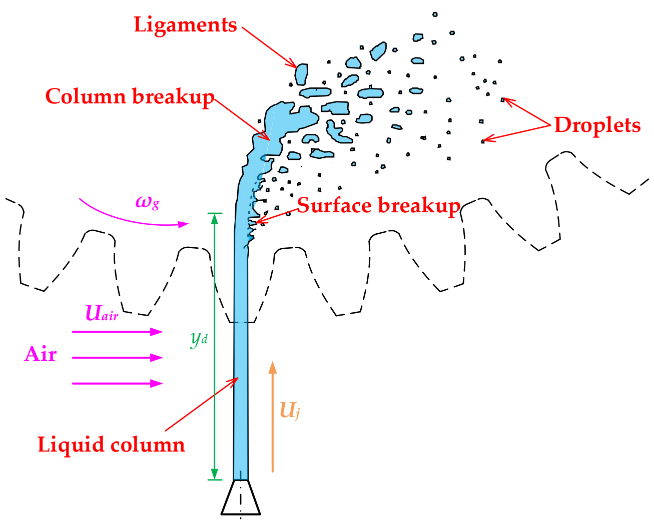

Figure 1. Sketch of a typical oil jet flow in an air crossflow.

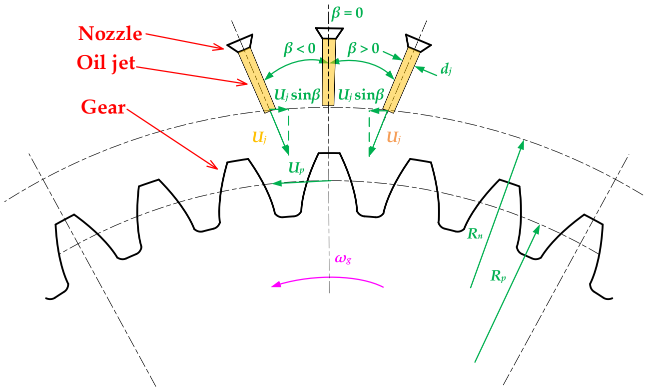

Figure 2. Sketch of oil jet lubrication and cooling.

2.3. Windage Resistance Torque

To quantify the oil jet losses generated by the oil jet hitting the gear teeth, it is desirable to extract the windage power losses from the total independent power losses for an isolated spur gear. A quasi-analytical windage power loss on the gear sides and teeth has been set up by Diab et al. [34], comparing favorably with experimental findings for different spur gears, as reported

$$P_w = \frac{1}{2} C_w \rho_{air} {\omega_g}^3 {R_a}^5 \tag{5}$$

or, the windage resisting torque

$$T_w = \frac{1}{2} C_w \rho_{air} {\omega_g}^2 {R_a}^5 \tag{6}$$

where $C_w = 2C_f + C_t$, where the nondimensional number of torque coefficient C_f on the front/rear faces is as follows:

$$C_f = \frac{2n_1\pi}{5-2m_1}\frac{1}{\mathrm{Re}^{*m_1}}\left(\frac{R^*}{R}\right)^5 + \frac{2n_2\pi}{5-2m_2}\left[\frac{1}{\mathrm{Re}^{m_2}} - \frac{1}{\mathrm{Re}^{*m_2}}\left(\frac{R^*}{R}\right)^5\right] \tag{7a}$$

where n_i and m_i: constant coefficient. i = 1, for laminar flows; i = 2, for turbulent flows. Re*($\approx 3 \times 10^{-5}$) is the critical Reynolds number to separate the laminar and turbulent flows and R^* is the corresponding critical radius. The nondimensional number of torque coefficient C_t on the gear teeth is as follows:

$$C_t \cong \xi \frac{Z}{4}\left(\frac{b_g}{R_p}\right)\left[1 + \frac{2(1+X_A)}{Z}\right]^4 (1-\cos\phi)(1+\cos\phi)^3 \tag{7b}$$

and

$$\phi = \pi/Z - 2(inv\alpha_p - inv\,\alpha_A) \tag{8}$$

where ξ is the reduction factor and X_A is the profile shift coefficient. α_P and α_A denote the pressure angle at the pitch and outside circle, respectively.

2.4. Wetted Length Tooth Surface

The lubricating oil injected from the nozzle hits the tooth surface and forms a film with the action of airflow. Impingement depth, oil film, and surface area are the most significant indicators to characterize lubrication and cooling performance. Following Kromer et al. [30,31], the impingement depth can be calculated. This study focuses on the situation where the oil jet angle β is set to zero. The impingement depth d_{imp} denotes the distance from the impact point of the oil jet flow on the gear flank to the outside circle (see

Figure 3). Regarding the gear center as its center, the gear angle θ_j between the base circle and an arbitrary point j on the gear surface is

$$\theta_j = \left[\left(\frac{R_j}{R_b}\right)^2 - 1\right]^{\frac{1}{2}} - \arccos\left(\frac{R_b}{R_j}\right) \tag{9}$$

where subscripts $_b$, $_o$, $_p$, $_r$, and $_{\text{imp}}$ represent the radius of base circle, outside circle, pitch circle, root circle, and impingement point, respectively. Then, the angle of the leeward side is

$$\theta_{lee} = \theta_o - \theta_r \tag{10}$$

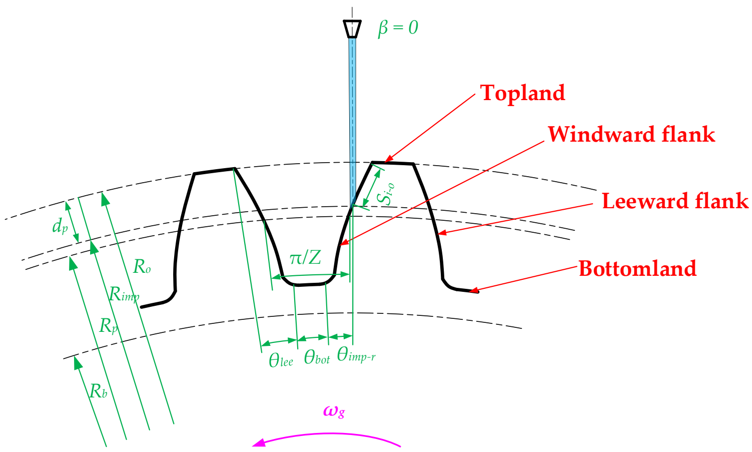

Figure 3. Schematic of the spur gear geometry under jet lubrication.

The gear angle of the bottomland can be calculated as

$$\theta_{bottom} = \frac{\pi}{Z} - 2(\theta_p - \theta_r) \tag{11}$$

The gear angle between the root radius and the impingement point on the windward side is expressed as

$$\theta_{imp-r} = \theta_{imp} - \theta_r \tag{12}$$

Subsequently, the total gear angle rotating from the time the oil flow reaches the addendum until it hits on the gear with the maximum depth is

$$\theta_{tot} = \theta_{lee} + \theta_{bottom} + \theta_{imp-r} \tag{13}$$

Meanwhile, the flying distance of the oil jet can be determined as

$$F = R_o - R_{imp} \tag{14}$$

Using Equations (13) and (14), the rotating speed of the gear is

$$n = \frac{30U_j\theta_{tot}}{\pi F} \tag{15}$$

One restriction for determining the impingement depth is that the impingement point cannot exceed the tooth depth on the windward side. In other words, the radius of the impingement points between the root radius and outside radius. Furthermore, the impingement depth can be calculated using a bisection method.

Whereafter, the arc length s_{i-o} of the oil film on the spur gear can be defined as

$$s_{i-o} = \frac{R_o{}^2 - R_{imp}{}^2}{2R_b} \tag{16a}$$

By multiplying with the teeth number and rotating speed, the arc length per unit time is

$$\dot{s}_{i-o} = \frac{n s_{i-o} Z}{60} \tag{16b}$$

With an empirical model developed by Guo [35], the width of the film at the moment the oil jet hitting the gear surface can be expressed as

$$W_{film} = 0.359 d_j \left(\frac{U_j}{\dot{s}_{i,o}}\right)^{\frac{1}{2}} \left(\frac{\rho_{oil} U_j d_j}{\mu_{oil}}\right)^{\frac{1}{2}} \tag{17}$$

In this study, the width of the film W_{film} cannot exceed the tooth width b_g, namely, $W_{film} \leq b_g$.

The wetted surface on the windward side is the product of the arc length and the width of the film, and can be described as

$$A_{film} = s_{i-o} W_{film} \tag{18}$$

3. CFD Modeling

The aim of this paper is to study the process by the action of lubricating oil impacting the rotating gear. To achieve this goal, the complicated gear train was simplified down to an isolated gear with a nozzle, and the bearings, shaft, and seals were ignored.

3.1. Geometry

A representative spur gear with an entire 360° geometry was defined, using the attributes as summarized in Table 1. The nozzle exit of the oil jet was directed radially (β = 0), located at a small distance of 12.5 mm from the addendum circle, as discussed in Section 2.1.

Table 1. Main physical properties of the modeled gear.

Variable	Symbol	Value
teeth number	Z	38
jet diameter	d_j	1 mm
gear width	b_g	10 mm
gear pitch diameter	d_p	126.7 mm
pressure angle	α_p	20°
distance from nozzle exit to the gear outside diameter	l_o	12.5 mm

An assumed temperature of 25 °C at atmospheric pressure was set as the operating temperature in this study, and the model was isothermal. Hence, the density and viscosity of lubricating oil are 889 kg/m^3 and 1.06 kg/ms, respectively. The density and viscosity of air are 1.225 kg/m^3 and 1.7894 × 10^{-5} kg/ms, respectively. The surface tension is 0.07 N/m.

3.2. Computational Domains and Numerical Setup

The overset mesh method provides unique advantages for the rotating motion of complex objects in many cases [36,37]. The overset mesh technology was exploited to achieve the rotating of the spur gear. A sketch of the simplified computational domain of the isolated gear with an oil jet nozzle, as depicted in Figure 4, includes two parts: one is the component domain wrapping the isolated spur gear, and the other is the background domain for the whole fluid field arranged an oil jet nozzle. More descriptions can be referred to in [33].

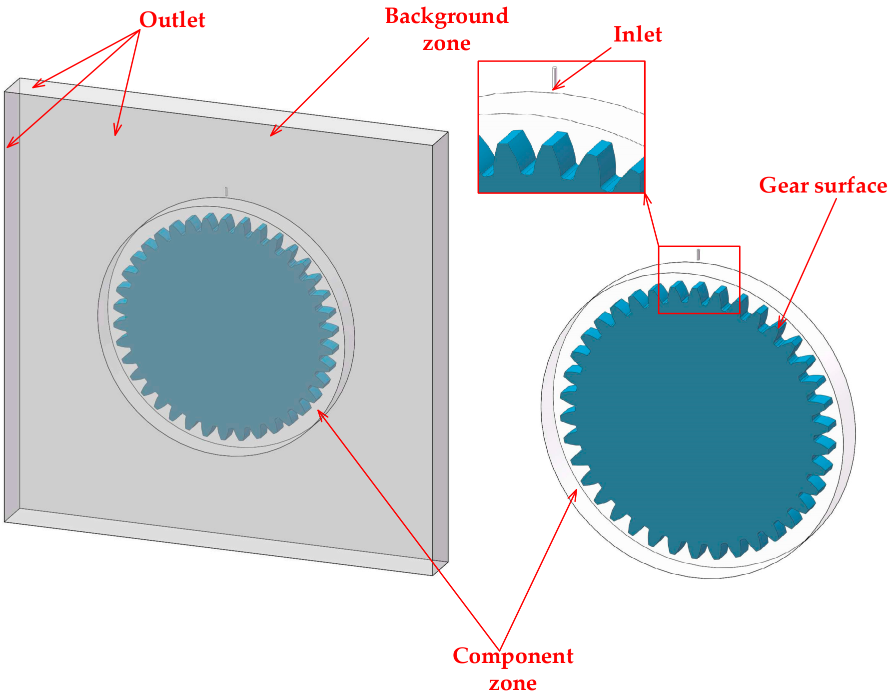

Figure 4. Computational domain of the spur gear.

As shown in Figure 4, the boundary condition of the velocity inlet was applied to the nozzle exit located in the background zone, while the pressure outlet was imposed on the outside surfaces of the background zone. All walls were set as the no-slip condition. All surfaces of the spur gear were defined as a whole, and the component zone wrapping the spur gear was rotating. ANSYS Mesh was adopted to divide tetrahedral meshes for the whole domains consisting of the component and background zone, as Figure 5 clearly shows. Most importantly, however, the size of the component mesh is very similar to that of the background. Local grid refinement in this study was imposed on the gear surfaces.

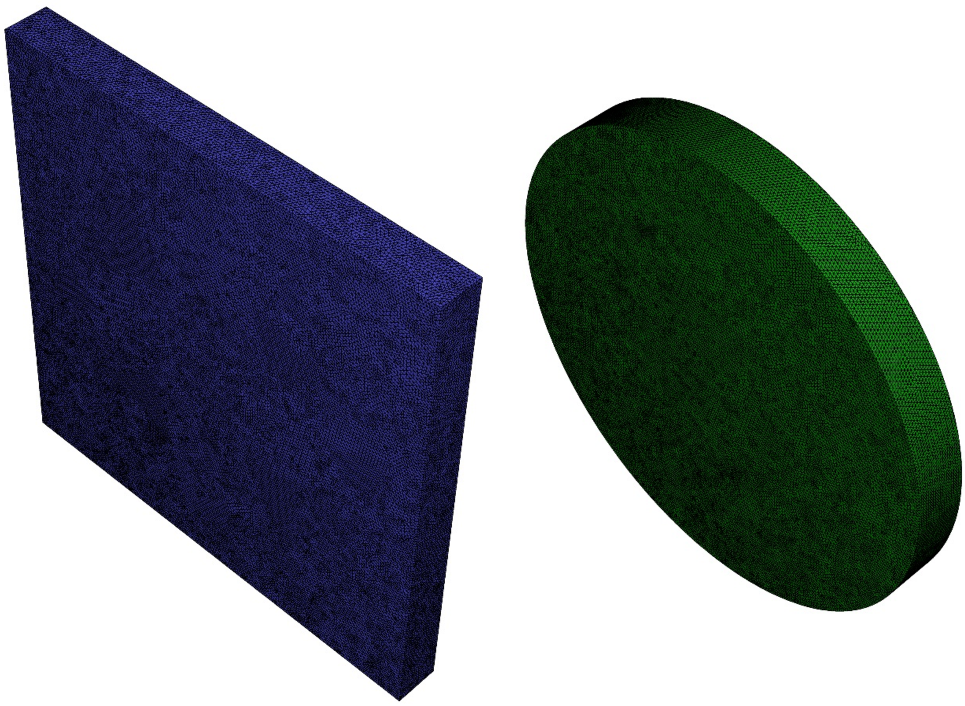

(**a**) (**b**)

Figure 5. Overset mesh topology: (**a**) background mesh; (**b**) component mesh.

A reliable commercial CFD software Fluent is introduced to address the oil–air two phase phenomenology of oil jet lubrication. The explicit VOF method was selected to study the oil–air two phase flow, the fluids were regarded as isothermal, and the air was treated as incompressible (Mach number < 0.3). The air and lubricating oil were defined as the primary and second phases, respectively. Their corresponding physical properties were described in the previous section. The SST k-ω turbulence model—currently most compatible for low Reynolds number flows—was adopted with the dimensionless wall parameter y+ less than 5. The scaled residuals were monitored and were less than 10^{-4} for every equation.

To determine the suitable element size and subtract the windage resisting moment, a mesh independence analysis was conducted by comparing the theoretical moments of the spur gear calculated from Equation (6) at the rotating speed of 9000 r/min. The numerical results of different mesh elements are summarized in Table 2. Compared with the theoretical resisting torque (T_w = 0.0911 Nm, at 9000 r/min) obtained by Equation (6), the numerical values including pressure and viscosity contribution exerting on the gear surfaces decrease by 4.83% from coarser to medium (from group 1 to 3), while they only increase by 1.54% from medium to dense. Consideration is given to the fact that the oil–air two phase flows would acquire a denser mesh, thus the dense-size grid in group 4 was preferred in this study. In addition, this study aims to quantitatively analyse the oil jet resistance torque with subtracting the windage resistance torque from the total resistance torque. In fact, the total time of the actual gear rotation in numerical investigations in this study is too short to form the air–lubricant mixture surrounding the gear; therefore, the fluid surrounding the gear can be regarded as pure air.

Table 2. Numerical results of resisting torque versus mesh element.

Group	Mesh Elements	Resisting Torque	Error
1	2,601,757	0.0970 Nm	6.48%
2	3,199,241	0.0982 Nm	7.79%
3	7,950,886	0.0926 Nm	1.65%
4	9,250,270	0.0912 Nm	0.11%

4. Results and Discussion

4.1. Comparison with Experimental Findings

As shown in Figure 6, the oil jet resistance torques calculated by Equation (4b) for the spur gear (m = 3 mm, Z = 42, b_g = 20 mm) are compared with experimental findings given by Ariura et al. [10]. Ignoring a few points at a low oil flow rate where experimental uncertainties are highest, the calculations coincide well with the experimental values, especially for high pitch line velocity and oil flow rate. Therefore, this study is concerned mainly with the case of oil jet lubrication with high pitch line velocity (about 40 m/s) and oil jet lubrication (over 20 m/s). In addition, the comparison indicated that the oil jet resistance torque is mostly caused by the power required to change the direction of the oil flow and reaccelerate it. The comparison also suggests that Equation (4b) can be used to predict the oil jet resistance torque.

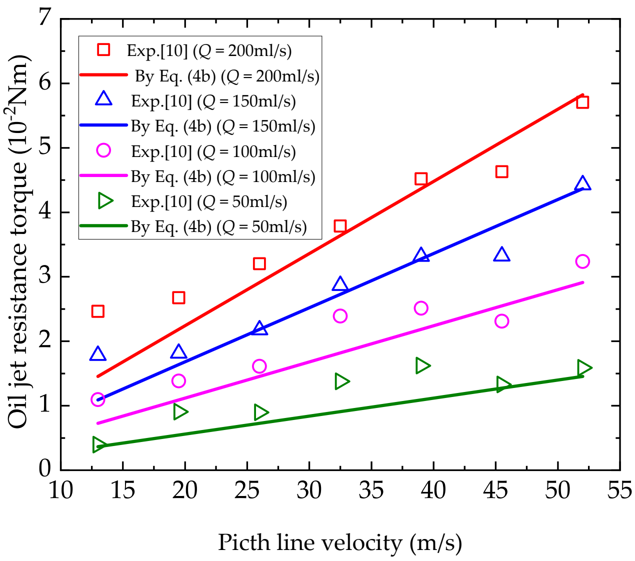

Figure 6. Calculations of oil jet resistance torque against pitch line velocity.

4.2. Prediction of Oil Jet Loss

The numerical investigations were performed with a fixed time step with a rotating speed n of 6000 r/min and oil jet velocity U_j of 20 m/s, that is to say, $U_j/U_p \approx 0.50$. Limited by the computational efforts, the simulations were stopped as the torque peak showed little fluctuation within 8%. The resisting torque changing with the rotating time is depicted in Figure 7. The calculation time of the numerical investigations is about 8 h and 20 min on our own Workstation (AMD EPYC 7302 16-Core Processor, 3.00 GHz). Every peak in Figure 7a is related to an impact process of oil jet flow on the gear tooth. It is found that, in the first quarter of the period, the impacts suffer from start-up effects, while they subsequently change little. Removing the volatile data at the beginning, the numerical torque from 2.372 ms to 3.668 ms was left, as shown in Figure 7b.

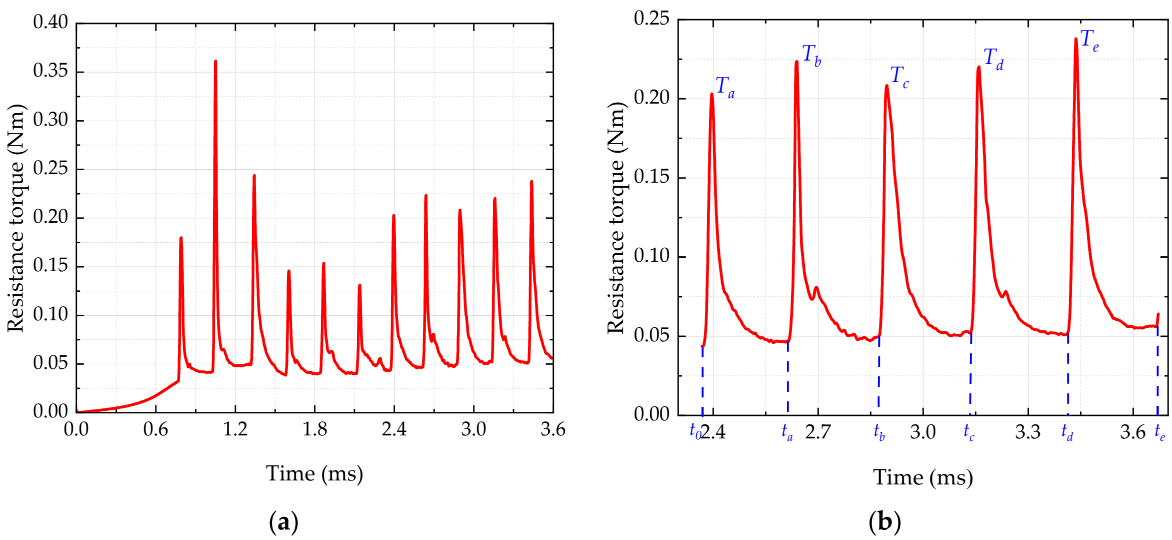

Figure 7. Resistance torque–time curve: (**a**) [0, 3.668 ms]; (**b**) [2.372 ms, 3.668 ms].

Divided by the theoretical resistance torque T_0 (0.0352 Nm) calculated from Equation (4), the main torque values in Figure 7b are listed in Table 3. The average time interval Δt is about 0.2592 ms, while the theoretical impact time per tooth $60/(n * Z)$ is 0.2631 ms. The oil jet hitting the tooth flank happens in a flash, and the momentum transfer between the oil jet flow and the gear surface occurs in a very short time, leading to a resistance torque peak.

Table 3. Main torque peak values (n = 6000 r/min, U_j = 20 m/s).

Time Node	Value	Torque Peak	Value
t_a	2.612 ms	T_a	5.765 T_0
t_b	2.872 ms	T_b	6.346 T_0
t_c	3.136 ms	T_c	5.920 T_0
t_d	3.412 ms	T_d	6.256 T_0
t_e	3.668 ms	T_e	6.734 T_0

The integral average value T_{avg} of total resistance torque in Figure 7b in the range of 2.372 ms to 3.668 ms is 0.0770 Nm. Subtracting the windage resistance torque T_w (0.0411 Nm), the net resistance torque resulting from the oil impacting the gear tooth is 0.0359 Nm. The absolute difference between the numerical and theoretical torque is 0.0007 Nm (corresponding power loss is 0.4398 W), while the relative difference is 1.99%. Calculation shows that the numerical results coincide well with analytical values for the case of the oil column hitting the gear surface without an obvious liquid breakup phenomenon. Meanwhile, at the rotating speed of 6000 r/min and oil jet speed of 20 m/s, the windage power loss (25.8297 W) is almost equal to the average oil jet loss (22.5566 W). Combining Equations (4)–(6), the oil jet loss is proportional to the rotating speed of the spur gear to the power two and the pitch radius of the gear to the power two, while windage loss is proportional to the rotating speed of the spur gear to the power three and the pitch radius of the gear to the power five. Predictably, the windage power loss rises faster than the oil jet loss with the increase in the rotating speed and pitch radius of the spur gear.

Moreover, the numerical investigations were also conducted with the rotating speed n of 6000 r/min and oil jet velocity U_j of 25 m/s, that is to say, $U_j/U_p \approx 0.63$. As before, the numerical torque from 2.568 ms to 3.888 ms is shown in Figure 7. Divided by the theoretical resistance torque T_0 (0.0440 Nm) calculated from Equation (4), the main torque values in Figure 8 are listed in Table 4.

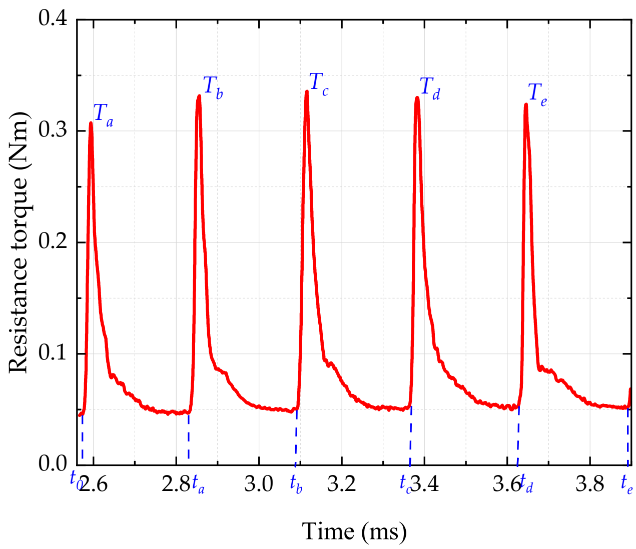

Figure 8. Resistance torque–time curve [2.568 ms, 3.888 ms].

Table 4. Main torque peak values (n = 6000 r/min, U_j = 25 m/s).

Time Node	Value	Torque Peak	Value
t_a	2.832 ms	T_a	6.986 T_0
t_b	3.092 ms	T_b	7.538 T_0
t_c	3.362 ms	T_c	7.631 T_0
t_d	3.622 ms	T_d	7.503 T_0
t_e	3.888 ms	T_e	7.365 T_0

The average time interval Δt of about 0.2628 ms is very close to the theoretical impact time per tooth $60/(n * Z)$ of 0.2631 ms. The integral average value Tavg of total resistance torque in Figure 8 in the range of 2.568 ms to 3.888 ms is 0.0878 Nm. Subtracting the windage resistance torque T_w (0.0411 Nm), the net resistance torque caused by the oil impacting the gear tooth is 0.0467 Nm. The resistance torque absolute difference and the relative difference are 0.0027 Nm and 6.14%, respectively. Combined with the above analysis, the theoretical resistance torques are actually somewhat below the numerical results. The main reasons for this are listed as follows. The range of airflow is about 1.0 and 1.5 times the gear radius, as in Figure 9. The closer to the spur gear, the larger the air velocity, especially in the tooth space. As the oil jet flow passes through the airflow surrounding the gear, the liquid column is accelerated to some extent. Meanwhile, as in Figure 1, the oil column does not breakup without ligaments and lots of droplets; the phenomenon of surface breakup still exists to produce a small number of droplets accelerated in the gear tooth space, and most of these drops finally impact the gear surfaces.

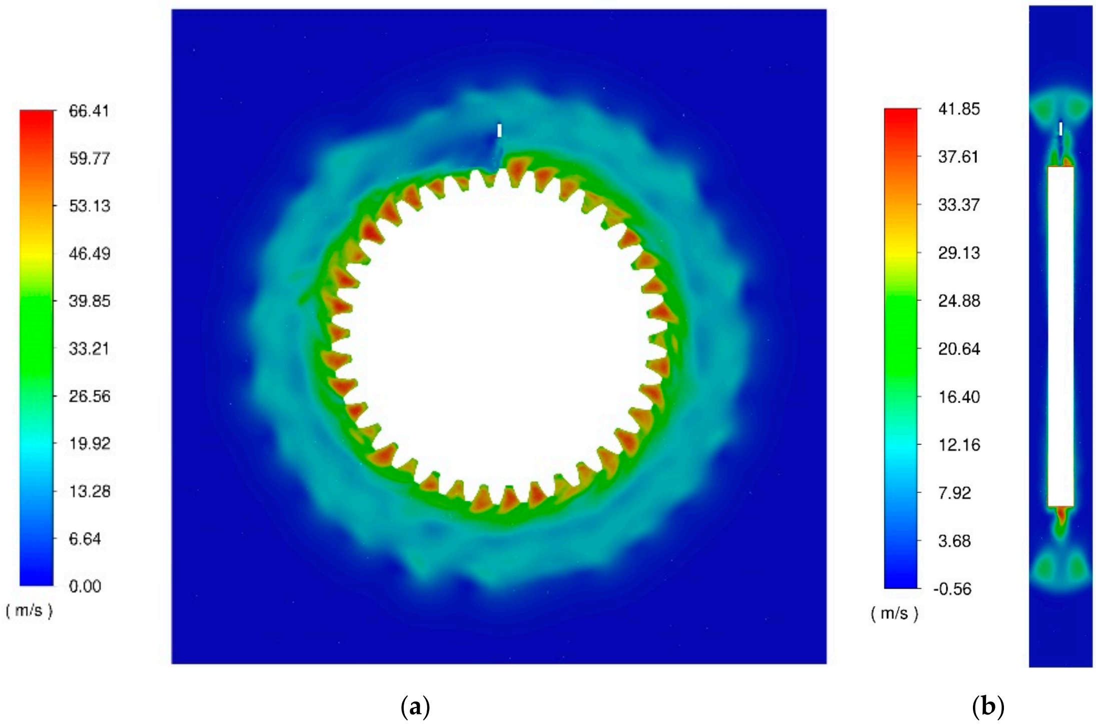

Figure 9. Velocity contour of the spur gear (n = 6000 r/min, U_j = 20 m/s): (**a**) velocity magnitude in front view; (**b**) tangential velocity in right view.

4.3. Wetting Behavior

First, the fourth typical impact period is recalled from Figure 7b. As illustrated in Figure 10, five characteristic points are used to make a concrete analysis. Correspondingly, the general observable jet flow of flow phenomenology is provided in Figures 10 and 11, while the wetting behavior of the oil film on the middle gear tooth is depicted in Figure 12.

Based on these five characteristic points, different flow phases distinguishable before and after the impacts on the middle gear tooth were searched for. First, at point 1 as shown in Figures 11a and 12a, the jet flow has cut off the interaction with the front tooth along the rotational direction and penetrated the tooth space between the preceding tooth and the current tooth. No obvious impact is observable. The resistance torque on the spur gear is only slightly above the windage resisting torque (see Figure 10), and the wetted surface on the middle tooth is nearly zero.

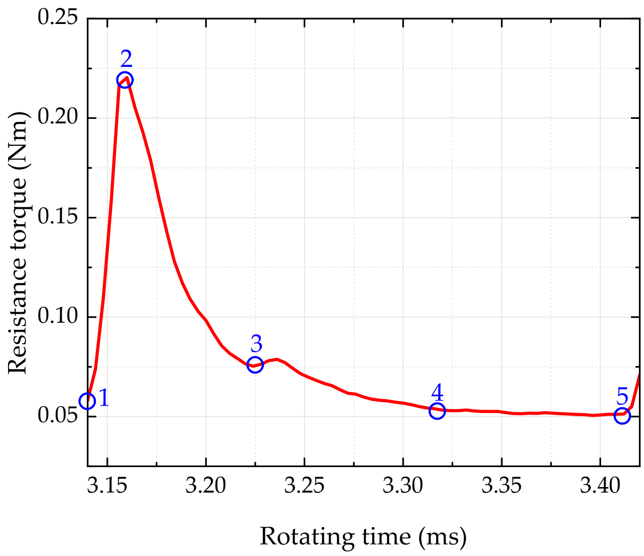

Figure 10. Resistance torque–time curve of typical impact process (n = 6000 r/min, U_j = 20 m/s).

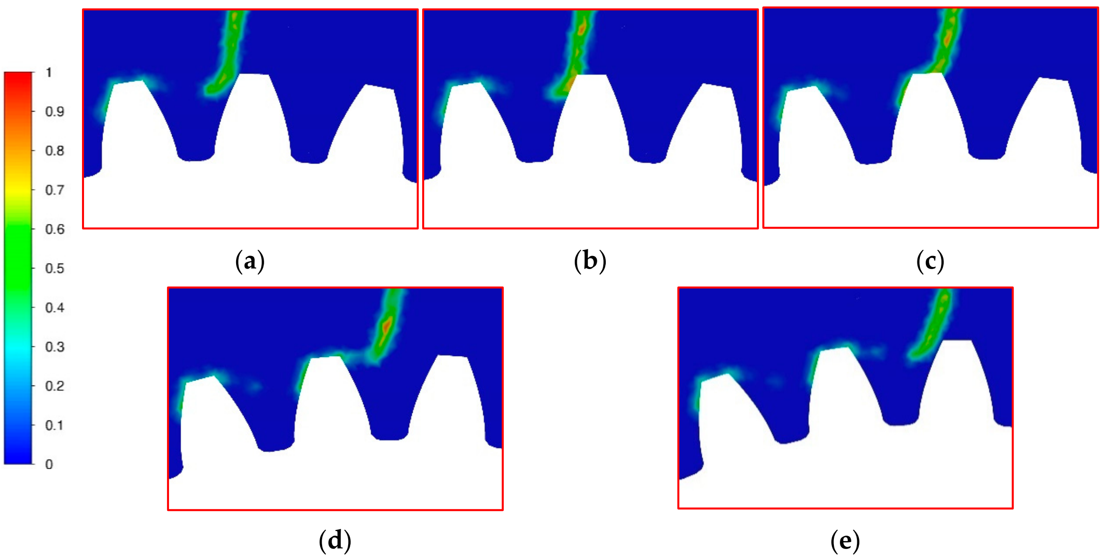

Figure 11. Volume fraction snapshots of the jet impingement at different time points (n = 6000 r/min, U_j = 20 m/s): (**a**) point 1; (**b**) point 2; (**c**) point 3; (**d**) point 4; (**e**) point 5.

Second, at point 2 as illustrated in Figures 11b and 12b, the impact between the jet flow and the gear surface occurs. The wetting behavior of the oil jet can be understood from three aspects—oil jet resistance torque, impingement depth, and wetted area. As can be seen from Figure 11b, the impact point reaches the deepest, where it recalls the well-known impingement depth as well as the radius of the impingement point; meanwhile, the resistance torque reaches its peak (see Figure 10). According to Section 2.3, the radius of the impingement point calculated using a bisection method is 63.9 mm, while the numerical radius by extracting the precise pixel coordinates in Figure 11b is about 64.6 mm; the difference is only 1.1%. Thus, the impingement depth is about 2.8 mm. Based on Equation (16), the arc length of the oil film on the spur gear is 3.1 mm. In accordance with Equation (18), the width of the film at the moment the oil jet hitting the gear surface is 1.9 mm, while the width by extracting the coordinates in Figure 12b is about 2.0 mm; the difference is only 5.26%. The wetted surface is approximately rectangle, thus the area on the basis of Equation (19) is 5.89 mm^2.

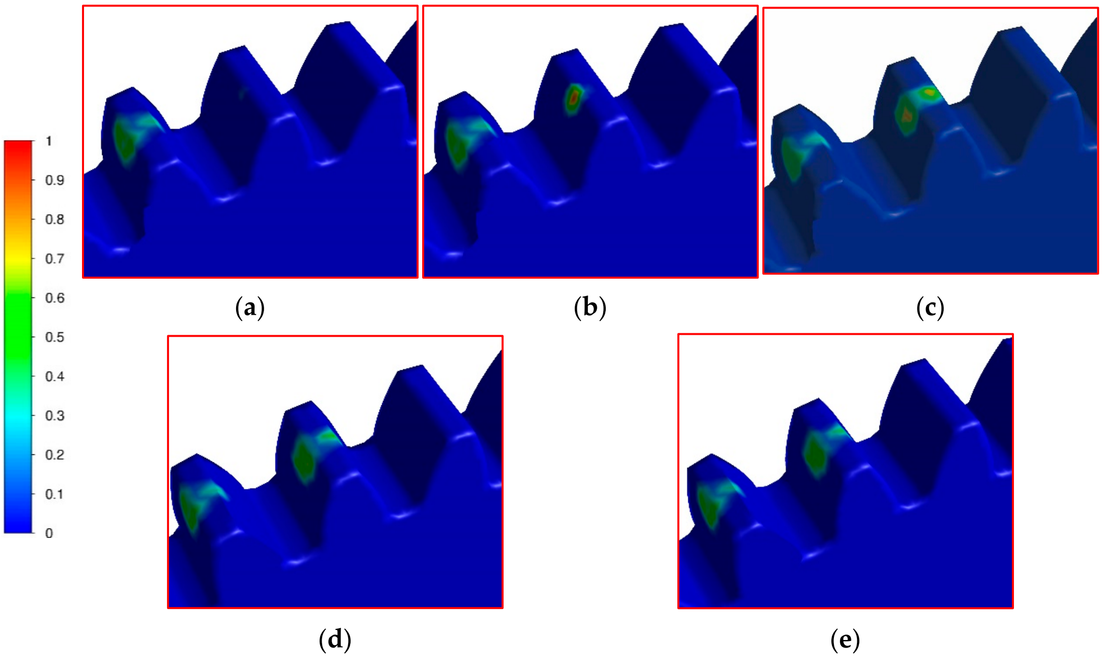

Figure 12. Volume fraction snapshots of the wetting behavior at different time points (n = 6000 r/min, U_j = 20 m/s): (**a**) point 1; (**b**) point 2; (**c**) point 3; (**d**) point 4; (**e**) point 5.

Then, from point 3 to point 4, the jet flow impacts on the gear flank until it cut off the interaction with the current gear tooth. Once the impact started, the oil quickly splashes/spreads over the tooth, along with the rapid increase in the wetted area of the oil film until it reaches the maximum at point 4, as shown in Figures 11 and 12. In this case, around 37% of the gear width is covered with an oil film. No de-wetting phenomenon is observed, and small amounts of oil are still flung off without a doubt. This effect can be negligible in this study. Finally, at point 5 as illustrated in Figures 11e and 12e, the jet flow was completely away from the proceeding gear tooth, and was about to arrive at the latter gear tooth, similar to point 1.

5. Conclusions

A detailed investigation of the flow phenomenology of the jet flow impinging on the tooth surface of an isolated spur gear under oil jet lubrication is presented in this study. The related theoretical models are introduced to quantify the resistance torque, impingement depth, and wetted area of oil film on the gear flank, providing simple tools for rapidly estimating the jet lubrication behavior, particularly the oil jet resistance torque and initial wetting area of oil film. Not only that, an unstructured overset mesh technique integrated with the VOF method was used to investigate in detail the transient and spatial flow field characteristics of the oil jet impacts on the gear surface. The estimations calculated by theoretical models and numerical results show high consistency, with the deviation of the oil jet power loss around 6%, the radius of the impingement point about 1.1%, and the width of the oil film approximately 5.26%. In view of these, it is indicated that these physical models are sufficiently accurate to deeply understand the jet lubrication behavior. It is also suggested that the overset mesh method integrated with the VOF method can be regarded as one alternative to pursuing the research on oil jet lubrication behavior. Based on this study, on the one hand, the total no-load power loss generated from the impact behavior of the oil jet flow on the gear flank and the windage behavior can be quickly and effectively predicted, and this can offer a theoretical basis in the thermal design of the gearing system; on the other hand, the estimation of the initial wetting area of oil film on the gear surface can provide a valuable reference for improving the lubrication and cooling performance of spur gears.

However, this study only concerns the impacts of the liquid column of an oil jet flow on an isolated spur gear under jet lubrication. Further work can be done to investigate the complex oil jet–gear interaction flow phenomenon in a spiral bevel gear-pair, with oi jet liquid column breakup in consideration.

Author Contributions: Conceptualization, X.Z. and Y.D.; methodology, C.L.; software, X.Z.; validation, X.Z.; formal analysis, C.L.; investigation, C.L.; resources, Y.D.; data curation, X.C.; writing—original draft preparation, X.Z.; writing—review and editing, X.Z.; visualization, X.Z.; supervision, Y.D.; project administration, Y.D.; funding acquisition, Y.D. All authors have read and agreed to the published version of the manuscript.

Funding: This research was funded by the National Defense Preliminary Research Project of China, grant number KY-44-2018-0219.

Acknowledgments: We would like to express our thanks to the editors of Lubricants and the anonymous reviewers for their work in processing this article.

Conflicts of Interest: The authors declare no conflict of interest.

Nomenclature

A_{film}	wetted surface of the oil film on the windward side [m^2]
b_g	gear width [m]
C_f	nondimensional number of torque coefficient on the front/rear faces
C_t	nondimensional number of torque coefficient on the gear teeth
C_w	nondimensional number of windage resisting torque
d_p	gear pitch diameter [m]
d_{imp}	impingement depth [m]
d_j	jet diameter [m]
F	flying distance of the oil jet [m]
$inv\ \alpha_P$, $inv\ \alpha_A$	involute function
l_o	distance from the nozzle exit to the gear outside diameter [m]
n	rotating speed of the gear [r/min]
n_i, m_i	constant coefficient. i = 1, for laminar flows; i = 2, for turbulent flows
P_w	windage power loss [W]
q	oil to air momentum ratio
Q	rate of oil flow [m^3/s]
R^*	critical radius to separate the laminar and turbulent flows [m]
R_a	outside radius [m]
R_b	base radius [m]
Re*	critical Reynolds number to separate the laminar and turbulent flows
R_n	radius of the nozzle exit [m]
R_o	outside radius [m]
R_p	pitch radius [m]
$s_{i\text{-}o}$	arc length of the oil film [m]
$\dot{s}_{i-o}$	arc length of the oil film per unit time [m/s]
T_0	oil jet resistance torque (β = 0) [N·m]
T_j	oil jet resistance torque [N·m]
T_w	windage resisting torque [N·m]
U_{air}	circumferential airflow velocity [m/s]
U_j	oil jet velocity [m/s]
U_p	pitch line velocity [m/s]
W_{ecf}	Weber number
W_{film}	width of the film [m]
X_A	profile shift coefficient
y_d	calculated travel distance of the oil flow [m]
Z	teeth number
α_P, α_A	pressure angle at the pitch and outside circle, respectively [rad]
β	oil jet angle [rad]

θ_{bottom}	gear angle of the bottomland [rad]
θ_{imp}	gear angle between the base circle and the circle of the impingement point [rad]
$\theta_{imp\text{-}r}$	gear angle between the root radius and the impingement point on the windward side [rad]
θ_j	gear angle between the base circle and an arbitrary point *j* on the gear surface [rad]
θ_{lee}	gear angle of the leeward side [rad]
θ_o	gear angle between the base circle and outside circle [rad]
θ_p	gear angle between the base circle and pitch circle [rad]
θ_r	gear angle between the base circle and root circle [rad]
θ_{tot}	total gear angle rotating from the time the oil flow reaches the addendum until hits on the gear [rad]
μ_{oil}	oil viscosity [Pa·s]
ξ	reduction factor
ρ_{air}	air density [kg/m^3]
ρ_{oil}	oil density [kg/m^3]
σ	surface tension coefficient of oil [N/m]
ω_g	angular velocity of the gear [rad/s]

References

1. Handschuh, R.R.; Kilmain, C.J. *Efficiency of High-Speed Helical Gear Trains*; Technical Report NASA/TM-2003-212222; ARL-TR-2968; Cleveland OH Glenn Research Center: Cleveland, OH, USA, 2003.
2. Eastwick, C.N.; Johnson, G. Gear windage: A review. *J. Mech. Des.* **2008**, *130*, 034001. [CrossRef]
3. Seetharaman, S.; Kahraman, A. Load-independent spin power losses of a spur gear pair: Model formulation. *J. Tribol.* **2009**, *131*, 022201. [CrossRef]
4. Hu, X.; Wang, A.; Li, P.; Wang, J. Influence of dynamic attitudes on oil supply for bearings and churning power losses in a splash lubricated spiral bevel gearbox. *Tribol. Int.* **2021**, *159*, 106951. [CrossRef]
5. Boni, J.B.; Changenet, C.; Ville, F. Analysis of flow regimes and associated sources of dissipation in splash lubricated planetary gear sets. *J. Tribol.* **2021**, *143*, 111805. [CrossRef]
6. Quiban, R.; Changenet, C.; Marchesse, Y.; Ville, F. Experimental investigations about the power loss transition between churning and windage for spur gears. *J. Tribol.* **2021**, *143*, 024501. [CrossRef]
7. Maccioni, L.; Concli, F. Computational fluid dynamics applied to lubricated mechanical components: Review of the approaches to simulate gears, bearings, and pumps. *Appl. Sci.* **2020**, *10*, 8810. [CrossRef]
8. Talbot, D.; Kahraman, A.; Seetharaman, S. A helical gear pair pocketing power loss model. *J. Tribol.* **2014**, *136*, 021105. [CrossRef]
9. Ruzek, M.; Marchesse, Y.; Ville, F.; Velex, P. Windage power loss reductions in high-speed gear pairs. *Forsch. Ing.* **2019**, *83*, 387–392. [CrossRef]
10. Ariura, Y.; Ueno, T.; SunAGA, T.; Sunamoto, S. The lubricant churning loss in spur gear systems. *Bull. JSME* **1973**, *16*, 881–892. [CrossRef]
11. Chaari, F.; Romdhane, M.B.; Baccar, W.; Fakhfakh, T.; Haddar, M. Windage power loss in spur gear sets. *WSEAS Trans. Appl. Theor. Mech.* **2012**, *7*, 159–168.
12. Concli, F. Thermal and efficiency characterization of a low-backlash planetary gearbox: An integrated numerical-analytical prediction model and its experimental validation. *Proc. Inst. Mech. Eng. Part J J. Eng. Tribol.* **2016**, *230*, 996–1005. [CrossRef]
13. Mastrone, M.N.; Hartono, E.A.; Chernoray, V.; Concli, F. Oil distribution and churning losses of gearboxes: Experimental and numerical analysis. *Tribol. Int.* **2020**, *151*, 106496. [CrossRef]
14. Concli, F.; Gorla, C. Analysis of the power losses in geared transmissions–measurements and CFD calculations based on open source codes. In Proceedings of the International Gear Conference 2014, Lyon, France, 26–28 August 2014; Elsevier Science & Technology: Amsterdam, The Netherlands, 2014. [CrossRef]
15. Akin, L.S. An interdisciplinary lubrication theory for gears (with particular emphasis on the scuffing mode of failure). *J. Eng. Ind.* **1973**, *95*, 1178–1195. [CrossRef]
16. Dai, Y.; Jia, J.; Ouyang, B.; Bian, J. Determination of an optimal oil jet nozzle layout for helical gear lubrication: Mathematical modeling, numerical simulation, and experimental validation. *Complexity* **2020**, *2020*, 2187027. [CrossRef]
17. Zhu, X.; Dai, Y.; Ma, F.; Ouyang, B. Mathematical modeling and numerical simulation for determining an optimized oil jet layout for spiral bevel gear lubrication. *Proc. Inst. Mech. Eng. Part J J. Eng. Tribol.* **2021**, *235*, 611–628. [CrossRef]
18. Dai, Y.; Ma, F.; Zhu, X.; Su, Q.; Hu, X. Evaluation and optimization of the oil jet lubrication performance for orthogonal face gear drive: Modelling, simulation and experimental validation. *Energies* **2019**, *12*, 1935. [CrossRef]
19. Zhu, X.; Dai, Y.; Ma, F. CFD modelling and numerical simulation on windage power loss of aeronautic high-speed spiral bevel gears. *Simul. Model. Pract. Theory* **2020**, *103*, 102080. [CrossRef]
20. Zhu, X.; Dai, Y.; Ma, F. On the estimation of the windage power losses of spiral bevel gears: An analytical model and CFD investigation. *Simul. Model. Pract. Theory* **2021**, *110*, 102334. [CrossRef]

21. Liu, J.; Ni, H.; Xu, Z.; Pan, G. A simulation analysis for lubricating characteristics of an oil-jet lubricated ball bearing. *Simul. Model. Pract. Theory* **2021**, *113*, 102371. [CrossRef]
22. Karaca, H.D.; Ozen, G.D.; Kasnakoglu, C. Nonlinear modelling and control of the flow over aerofoils using CFD simulations. *Simul. Model. Pract. Theory* **2016**, *67*, 29–43. [CrossRef]
23. Concli, F.; Gorla, C.; Della Torre, A.; Montenegro, G. Windage power losses of ordinary gears: Different CFD approaches aimed to the reduction of the computational effort. *Lubricants* **2014**, *2*, 162–176. [CrossRef]
24. Concli, F.; Gorla, C. Numerical modeling of the power losses in geared transmissions: Windage, churning and cavitation simulations with a new integrated approach that drastically reduces the computational effort. *Tribol. Int.* **2016**, *103*, 58–68. [CrossRef]
25. Fondelli, T.; Andreini, A.; Da Soghe, R.; Facchini, B.; Cipolla, L. Numerical simulation of oil jet lubrication for high speed gears. *Int. J. Aerosp. Eng.* **2015**, *2015*, 752457. [CrossRef]
26. Massini, D.; Fondelli, T.; Facchini, B.; Tarchi, L.; Leonardi, F. Experimental investigation on power losses due to oil jet lubrication in high speed gearing systems. In Proceedings of the ASME Turbo Expo 2017: Turbomachinery Technical Conference and Exposition. Volume 50886: Heat Transfer, Charlotte, NC, USA, 26–30 June 2017. [CrossRef]
27. Keller, M.C.; Kromer, C.; Cordes, L.; Schwitzke, C.; Bauer, H.J. CFD study of oil-jet gear interaction flow phenomena in spur gears. *Aeronaut. J.* **2020**, *124*, 1301–1317. [CrossRef]
28. Keller, M.C.; Braun, S.; Wieth, L.; Chaussonnet, G.; Dauch, T.; Koch, R.; Höfler, C.; Bauer, H.J. Numerical modeling of oil-jet lubrication for spur gears using smoothed particle hydrodynamics. In Proceedings of the 11th International SPHERIC Workshop, Munich, Germany, 14–16 June 2016.
29. Keller, M.C.; Braun, S.; Wieth, L.; Chaussonnet, G.; Dauch, T.F.; Koch, R.; Schwitzke, C.; Bauer, H.J. Smoothed particle hydrodynamics simulation of oil-jet gear interaction1. *J. Tribol.* **2019**, *141*, 071703. [CrossRef]
30. Kromer, C.; von Plehwe, F.C.; Keller, M.C.; Schwitzke, C.; Bauer, H.J. Analytical model for the heat transfer in impingement cooled spur gears. In *Turbo Expo: Power for Land, Sea, and Air*; American Society of Mechanical Engineers: New York, NY, USA, 2020; Volume 84058, p. V001T01A023. [CrossRef]
31. Kromer, C.; von Plehwe, F.; Cordes, L.; Schwitzke, C.; Bauer, H.J. *Heat Transfer by Impingement Cooling of Spur Gears*; Deutsche Gesellschaft für Luft-und Raumfahrt-Lilienthal-Oberth eV: Bonn, Germany, 2020.
32. Wu, P.K.; Kirkendall, K.A.; Fuller, R.P.; Nejad, A.S. Breakup processes of liquid jets in subsonic crossflows. *J. Propul. Power* **1997**, *13*, 64–73. [CrossRef]
33. Wu, P.K.; Kirkendall, K.A.; Fuller, R.P.; Nejad, A.S. Spray structures of liquid jets atomized in subsonic crossflows. *J. Propul. Power* **1998**, *14*, 173–182. [CrossRef]
34. Diab, Y.; Ville, F.; Velex, P.; Changenet, C. Windage losses in high speed gears-preliminary experimental and theoretical results. *J. Mech. Des. Trans. ASME* **2004**, *126*, 903–908. [CrossRef]
35. Guo, Y. Newtonian and Viscoelastic Liquid Jet Impingement on A Moving Surface. Master's Thesis, University of British Columbia, Vancouver, BC, Canada, 2014.
36. Gao, Z.; Wang, Y.; Su, Y.; Chen, L. Validation of a combined dynamic mesh strategy for the simulation of body's large amplitude motion in wave. *Ocean Eng.* **2019**, *187*, 106169. [CrossRef]
37. Dai, Y.; Xu, L.; Zhu, X.; Ouyang, B. Application of an unstructured overset method for predicting the gear windage power losses. *Eng. Appl. Comput. Fluid* **2021**, *15*, 130–141. [CrossRef]